Steel and Composite Structures, *Vol. 32, No. 2 (2019) 265-279*
DOI: https://doi.org/10.12989/scs.2019.32.2.265

Application of self-centering wall panel with replaceable energy dissipation devices in steel frames

Sisi Chao, Hanheng Wu*, Tianhua Zhou, Tao Guo and Chenglong Wang

School of Civil Engineering, Chang'an University, Xi'an 710061, China

(*Received March 21, 2019, Revised May 17, 2019, Accepted June 1, 2019*)

Abstract. The self-centering capacity and energy dissipation performance have been recognized critically for increasing the seismic performance of structures. This paper presents an innovative steel moment frame with self-centering steel reinforced concrete (SRC) wall panel incorporating replaceable energy dissipation devices (SF-SCWD). The self-centering mechanism and energy dissipation mechanism of the structure were validated by cyclic tests. The earthquake resilience of wall panel has the ability to limit structural damage and residual drift, while the energy dissipation devices located at wall toes are used to dissipate energy and reduce the seismic response. The oriented post-tensioned strands provide additional overturning force resistance and help to reduce residual drift. The main parameters were studied by numerical analysis to understand the complex structural behavior of this new system, such as initial stress of post-tensioning strands, yield strength of damper plates and height-width ratio of the wall panel. The static push-over analysis was conducted to investigate the failure process of the SF-SCWD. Moreover, nonlinear time history analysis of the 6-story frame was carried out, which confirmed the availability of the proposed structures in permanent drift mitigation.

Keywords: steel frame; self-centering; energy dissipation devices; residual drift; lateral-force resistance

1. Introduction

The steel moment frame system has limited lateral stiffness to meet the requirements of engineering application as a unique lateral force resisting system. Past earthquake events demonstrated the superior performance of buildings incorporating the structural walls as the primary lateral load resisting system. Therefore, the reduplicate lateral force resisting system composite of the steel frame with infill walls has recently received focused attention to creating more effective and economical seismic resistant solutions (Dall'Asta *et al*. 2017). Structure dominated by shear walls were made of reinforced concrete, steel plate, light-weight panel and masonry *et al*. (Hajjar 2002, Saari *et al*. 2004, Tong *et al*. 2005, El-Tawil *et al*. 2010, Zona *et al*. 2016 and Khoshnoud and Marsono 2016). In recent years, the new concept of earthquake resilient structures was presented (SPUR 2009) to quickly restore the function after an earthquake and minimizie the impact on normal life. The self-centering (SC) structures allow members to uplift and rock without residual deformation and bending after the earthquake by utilizing post-tensioned technology to provide restoring force mechanism. Compared with traditional systems, the SC structure has an intrinsic advantage of drift capacity with limiting damage and residual drift. Nowadays, the seismic performance of SC structures has been the focus of many experimental and numerical studies. Aaleti and Sritharan (2009) proposed a simplified method for characterizing monotonic behavior of precast wall systems. The elongation of post-tensioning steel was of critical importance for the design of systems incorporating unbonded post-tensioning. Chi and Liu (2012) investigated the cyclic response of a post-tensioned (PT) column base connection. The experiment demonstrated that the designed PT column base connections were able to withstand 4% story drift without structural damage and performed stable hysteretic behavior. Next, Deng *et al*. (2013) designed a beam-column connection for steel moment frames. The PT high-strength steel strands were also used along the beam. Though the connection has zero deformation after an earthquake and can be restored to their original status, the efficiency of such connections used in the whole steel frame still an important issue. Song *et al*. (2015a) introduced a new design form for prestressed shear walls with horizontal bottom slits utilizing cast-in-place technology. Due to the self-centering ability provided by unbonded prestressed tendons inside the wall, the flexural and shear deformations of the walls were substantially reduced. Meanwhile, the preliminary seismic approach of seismic-resistant self-centering rocking core system has been studied by Blebo and Roke (2015). This research also emphasized that the structure can be an effective lateral-force resisting system with more ductility. Then, Vetr *et al*. (2016) presented numerical studies on the rocking structure. The non-linear time-history analysis validated the superior seismic performance of medium-rise structure in small exceedance probabilities and minor damages in main structural members. Recently, Du *et al*. (2018) developed beam-through steel frames with self-centering modular

*Corresponding author, Associate Professor,
E-mail: wuhanheng@163.com

ISSN: 1229-9367 (Print), 1598-6233 (Online)

panels that overcome the unusual field construction of onsite post-tensioning. The nonlinear pushover analysis showed this structure could remain elastic up to 2% story drift and the panel columns could develop plastic hinges before yielding of the PT strands. However, confronted with the redundant large lateral displacement failure on main components, these structures were unable to dissipate energy during severe earthquake action.

Afterward, the application of energy dissipation devices in SC system is considered significant to improve the energy dissipation capacity. A beam-column connection with bottom flange friction devices was analyzed by Guo *et al*. (2011). The small residual displacement after each load cycle proved the good self-centering capacity. Due to the significant loss in the normal force of the bolts occurred after bolts bearing, the self-centering capacity was reduced. Rahgozar *et al*. (2016) also presented the self-centering controlled rocking systems are capable of reducing residual drift after severe earthquakes by swaying on their bases and concentrating damage in energy dissipation devices. Asgarian *et al*. (2016) studied the cyclic behavior of a self-centering hybrid damper, which was combined energy dissipating and re-centering components. The nonlinear dynamic analysis results emphasized the effective suppression of permanent displacement and peak interstory drifts. The excellent performance of uplift and rocking at wall base with minor damage were observed at large lateral drifts, consisting of small amounts of spalling in the wall toes. Then, the cyclic lateral load response of the PT concrete wall system was carried out by Henry *et al*. (2016). Twigden *et al*. (2017) investigated the cyclic response of post-tensioned concrete walls with varying amounts of supplemental damping. In company with the unbounded PT steel that anchored the foundation, the energy dissipater O-connectors were designed to jointing wall to end column. The test wall displayed good performance with uplift and rocking at wall base, but the minor damage was still observed in wall toe. Moreover, Ji *et al*. (2018) presented a hybrid coupled wall (HCW) system, the nonlinear dynamic analysis result showed that most of the damage was concentrated on coupling beams. Though the working effectiveness of energy dissipation devices was verified in the SC structures, local failure still occurred on major components of these structures, which lead to the instability of the structures.

1.1 SF-SCWD structural system

Among these studies, a steel moment frame with the replaceable reinforced concrete wall panel (SRW) structural system was proposed by Wu *et al*. (2016). The experimental results showed that the structures displayed two-phase failure mode, and it was recognized to reduce building damage under low-intensity earthquakes and enhance the ductility of the steel elements. However, the brittle failure on connection between steel frame and RC wall greatly reduced deformation capacity of the structure. To improve the seismic performance and deal with the problem of the brittle connection failure, the self-centering technology is applied in SRW structural system. An innovative steel moment frame system (SF) with self-centering SRC wall panel incorporating replaceable energy dissipation devices (SCWD) is presented here, where SCW represents the self-centering steel reinforced concrete wall panel, and D means the ED devices, as shown in Fig. 1. Most important components that make it different from traditional structures are parallel use of post-tensioned (PT) strands and replaceable ED devices, combined with SRC wall panels. The PT strands are the main component to provide re-centering mechanism for wall panel. The dampers supply energy dissipation mechanism through their yielding process in the structure.

The purpose of this paper is to evaluate the seismic behavior of the innovative steel frame with self-centering

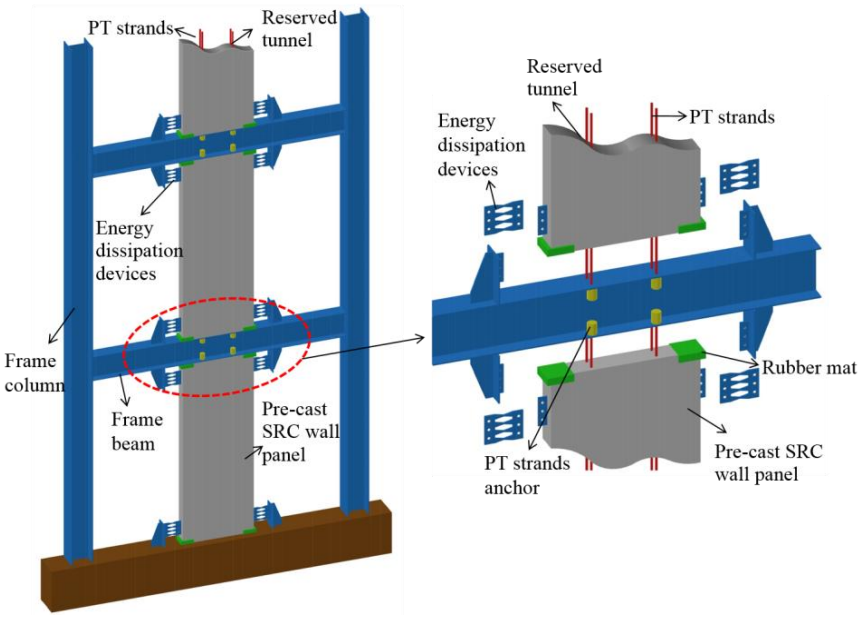

Fig. 1 SF-SCWD system

SRC wall panel. The cyclic test was conducted on the SCWD structure. The further experimental investigation and application of the proposed structures in seismic design, a reliable FEM analysis model was developed by ABAQUS to provide numerical modeling and its theoretic foundation. The details of the suggested simplified model, such as the element types, the material cyclic constitutive models, and the interactions between connections components were described. At the meantime, the parametric studies on PT strands, energy dissipation devices and wall dimensions were carried out to provide the reasonable suggestion to optimal self-centering performance and energy dissipation capacity. Besides, the static push-over analysis were performed to understand failure process of the multi-storey SF-SCWD frames. The nonlinear time-history analysis of 6-story SF-SCWD frames was conducted to evaluate the effectiveness in controlling lateral drift and residual deformation.

2. Cyclic loading tests on SCWD structure

A series of cyclic loading tests on SCWD structure have been successively performed by the research center for steel structures at Chang'an University (S-CHD). The complete test program is detailed in the S-CHD research reports (2019) and the summary of the test results is presented here. In order to validate the correctness of the finite element model, the general situation and cyclic test results on the sub-structure of SF-SCWD systems were briefly summarized.

2.1 Design principles of sub-structure

Under horizontal loading, the bending moment diagram of the new structures is shown in Fig. 2. It should be noted that there are four contra-flexural points, namely the bending moment is zero, located between the wall panel and beam-column joints. In order to clearly investigate mechanical properties of the self-centering wall panel and eliminate unnecessary impact of steel columns in the novel system, an analytical model mainly considering the self-centering wall panel was extracted from the structure. Accordingly, a piece of wall panel, together with the attached steel beams between contra-flexural points, was regarded as the basic analytical model. It is worth noted that the following basic assumptions are used in the analysis: (1) It is assumed that contra-flexural points are located at center positions of frame beams and RC wall panel; (2) The axial deformation of frame columns under horizontal load are small, and the vertical deformations on contra-flexural points of beams are mainly caused by axial deformation of frame beams. Therefore, the vertical deformations at frame columns and contra-flexural points are neglected. Based on the design principles of the sub-structure, the design performance objectives of the test specimens are determined in Fig. 3. PT strands keep elasticity and provide restore moment for the wall panel before 1/500 drift ratio. Afterward, the energy dissipators will yield firstly and completely prevent the plastic failure of the main load-bearing component until 1/50 drift ratio. After the earthquake, only energy dissipation devices need to be

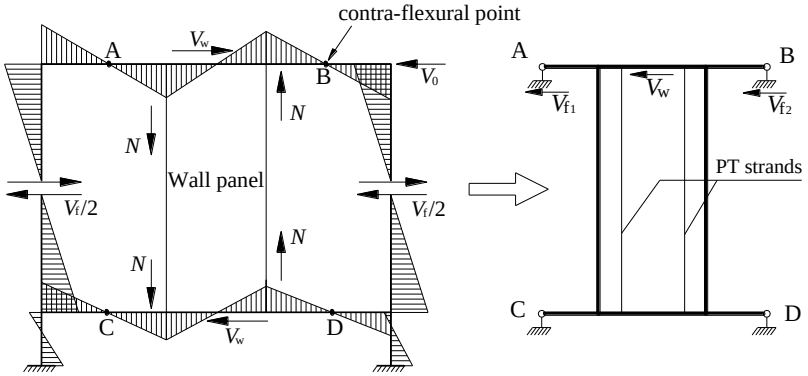

Fig. 2 Extraction of analytical model for SCWD sub-structure

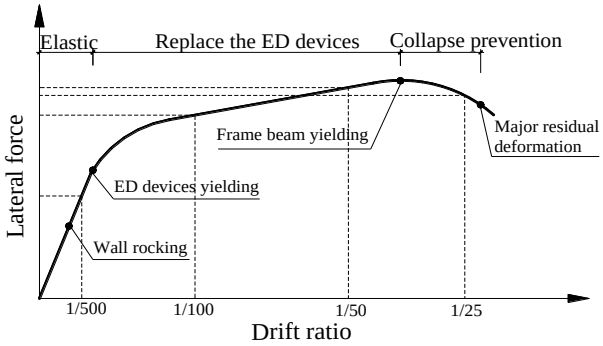

Fig. 3 The design objectives of SCWD sub-structure

replaced in continuing the work. Once the structure gets into the elastic-plastic deformation stage with major residual distortion on beams, the structures still have collapse prevention capacity.

2.2 Test program

2.2.1 Test specimen

The six test specimens were designed to have different level of PT initial stress and ED devices properties to study the influence of the two corporative mechanism. In this paper, the specimen with better energy dissipation capacity and self-centering performance was selected for a detailed introduction. The attached steel beams were fabricated using hot-rolled H-section steel, with the section of H400×200×8×13 and length of 2350 mm. The geometrical size of wall panel was 2450 mm (height) × 900 mm (width). The concrete used in the specimen has strength grade C40 with nominal cubic compressive strength f_c = 26.8 MPa. According to ACI 318M-14 (2014), the width of the wall was 160 mm that was greater than the minimum wall thickness 100 mm, and the height-length ratio of the rectangular wall panel was 2.83. In order to relieve the local stress concentration between wall corners and beams, the rubber mats were arranged on wall toes, along with the stiffening steel plates installed on beam webs. In addition, the embedded structural steel I120×74×5×8.4 were fully installed into the precast wall panel. It was used for connection between the frame beam and ED devices and ensured the wall panel has enough lateral stiffness. The frame beams have a strength grade of Q345 with f_y = 345 MPa, and the embedded structural steels have a strength grade of Q235.

As the component providing self-centering function, the unbonded post-tensioning strands in the duct were installed throughout the height of wall panel and anchored to the outer flanges of the beam, which have a cross-sectional area of 177 mm^2, the yield stress of 830 MPa, the ultimate stress of 1030 MPa and modulus of elasticity of 195 GPa. The initial stress of PT strands were defined as 40% of the ultimate strength. Besides, the ED devices were made of 8mm low-yield-point steel plates in shear type. Note that the energy dissipation devices were connected by bolts between non-embedded parts of section steel in walls and frame beams. The specimen configurations were shown in Fig. 4.

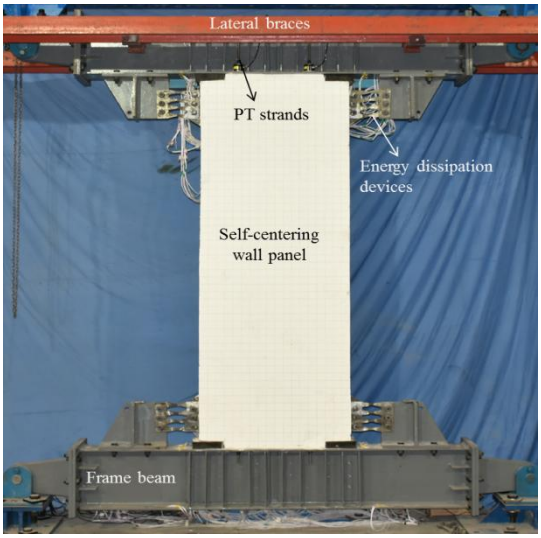

Fig. 4 Specimen configurations

2.2.2 Test setup and loading sequence

In order to accurately exert lateral force without additional vertical deformation, the L-shaped loading rigid girder was utilized in this test. The design of beam ends that determined as the hinge joints were to simulate the contra-flexural points. The specimen was fixed on L girder and foundation through the pinned connection between hinged parts and frame beams, as shown in Fig. 5. After the frame beams and wall panel located, then installed the energy dissipation devices. The lateral support beams were placed in front and back positions of frame beams to prevent torsion and instability of the specimens during the loading process. The lateral cyclic loads were applied by the horizontal actuator on a central position in the side of L girder.

The loading was applied using two steps in the test. Firstly, the strands were given to specify initial stress before lateral loading. This step also allowed the post-tensioning force transfer into frame beam as a pre-compression.

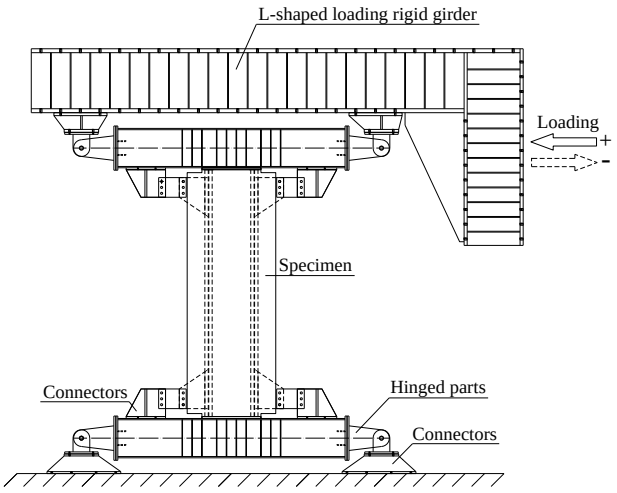

Fig. 5 Test setup

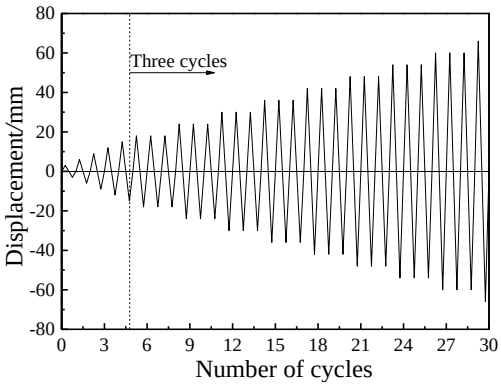

Fig. 6 Loading protocal

(a) Yielding of ED devices (b) Wall-beam gap opening (c) ED devices plastic deformation

Fig. 7 Typical deformation modes of SCWD structure

Secondly, the quasi-static cyclic loading with displacement control was adopted as depicted in Fig. 6. The loading direction was parallel to the length direction of L rigid beam. The lateral displacement loading began with 3 mm increment of the single cycle until the ED devices yielded. Subsequently, three fully reversed cycles with an increment of 6 mm were applied at each lateral displacement. When lateral displacement reached to 1/50 lateral drift ratio that exceeds the value satisfied to ACI ITG-5.1-07 (2007), then stops loading after a week of recirculation.

2.3 Test results and discussions

2.3.1 Failure mode

As displacement loading increased to 12 mm, relative separation between wall and beam become the first deformation mode, the self-centering wall panel displays rocking mechanism. The second typical deformation mode of SCWD sub-structure under cyclic loads is energy dissipation mechanism, which is characterized by the yielding of ED devices since 15 mm (Fig. 7(a)). As the load gradually increases to 36 mm, the ED plates were in the plastic phase and the measured values of strain gauges had exceeded 1000 $\mu\varepsilon$. The gap opening between the wall panel and beam increased to 8.5 mm at 42 mm displacement (1/100 drift ratio), as shown in Fig. 7(b). As expected, the elongation of PT strands caused an increase in the post-tensioning force, then led to higher bearing capacity of the specimen. The wall panel and beam still maintained elastic state during to 2% drift ratio and the plastic deformation of the structure mainly concentrates on ED devices (Fig. 7(c)). Contributed by excellent elastic deformability and certain vertical bearing capacity of the rubber mats, the wall panel returned to original undeformed position when unloading to zero. Besides, it also improved the safety of the structure and prevented the wall panel from the additional deformation caused by overturning moments.

2.3.2 Load-displacement response

The excellent self-centering performance with adequate energy dissipation capacity was observed in hysteretic response, as shown in Fig. 8. During the whole loading process, three limit states were indicated in the structure. In the OA loading stage for elastic stage, the components are completely elastic state, therefore the structural bearing capacity was linearly increased to 63.3 kN. The structural stiffness before wall rocking was 8.65 kN/mm. Due to the

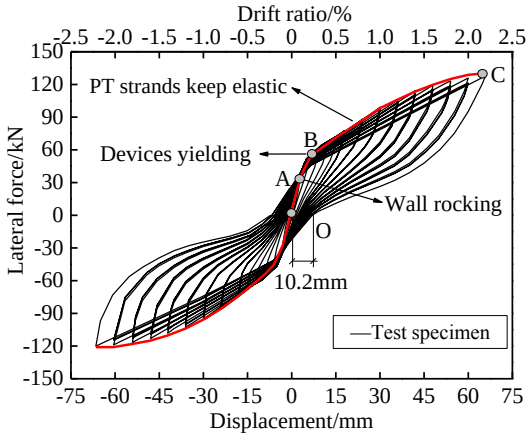

Fig. 8 Typical hysteresis curves of SCWD structure

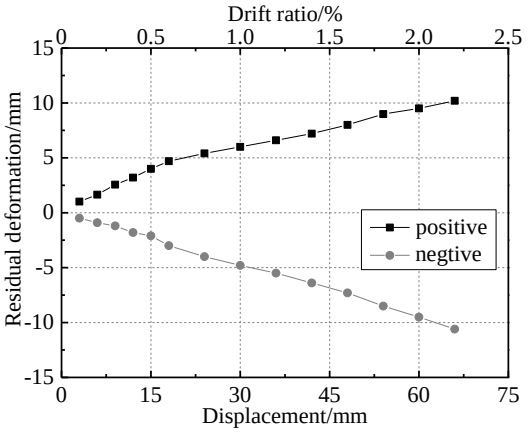

Fig. 9 Residual deformation of specimen

ED devices subjected to shear force, the structural stiffness was slightly reduced In the AB segment. Correspondingly, the uplift of wall corner became clearly visible at 0.2% drift angle. Rotation of the wall elongated the PT strands tensioning and also increased the strain on the devices. Despite devices had completely yielded at 0.5% drift ratio, the other components in this structure were still in an elastic state owing to the elasticity of PT strands. In the BC segment, the stiffness reduced to 1.77 kN/mm. The structural stiffness was decline rapidly after the yielded of ED devices. The structure achieved greater force capacity during the cycles to 2% lateral drift, the peak force 130.31 kN was reached at the last cycle. Fig. 10 shows the residual

Table 1 Material properties of steel

Location	Yield strength f_y(MPa)	Ultimate strength f_u(MPa)	Modulus of elasticity E_0 (MPa)	Elongation δ/%
Web of H beam	311.9	464.5	2.20×10^5	28
Flange of H beam	298.1	460.8	2.14×10^5	30
Energy dissipation devices	105.7	248.0	1.97×10^5	53.7
PT strands	860	1080	1.95×10^5	10

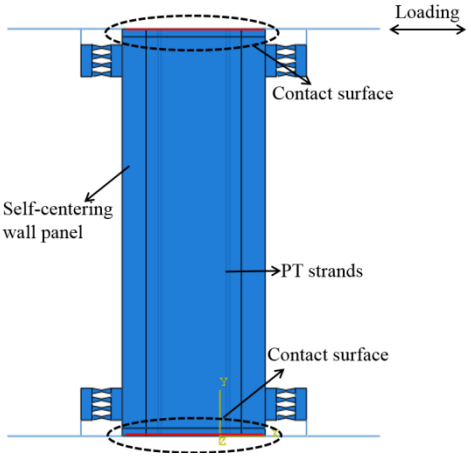

Fig. 10 Assembly model of BASE specimen

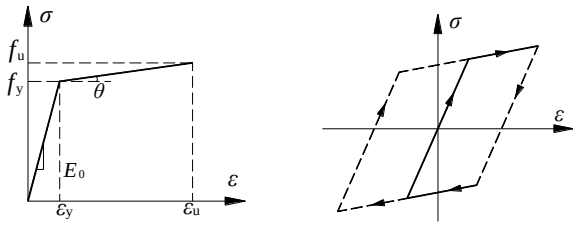

Fig. 11 Stress-strain relationship of steel

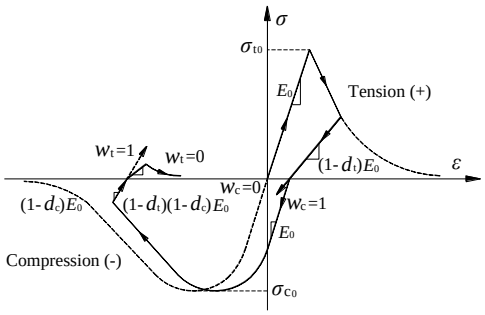

Fig. 12 Stress-strain relationship of concrete

deformation of the specimen at each drift ratio. Under lateral loading, residual deformation Δ_r increased in steady-state. The maximum residual deformation was 10.2 mm at 2% drift ratio, which only accounted for 0.35% of the specimen layer height. As a result, the unbonded post-tensioned precast wall panel has enough strength and stiffness that provide adequate lateral force resistance for the structure.

3. Numerical analysis on SF-SCWD sub-structure

3.1 Numerical model development

In order to simplify the load-deformation response of the SCWD system, a planer finite element model was developed by ABAQUS (2011), as shown in Fig. 10. The designed analytical model is labeled as the BASE. As the shear-type energy dissipation devices were adopted in the test specimen, the flexural type devices also analyzed in numerical research. Besides, the PT strands ultimate stress of 1030 MPa and modulus of elasticity of 195 GPa The numerical model utilized three different steel material definitions for various elements in the Specimen BASE, including PT strands, steel frame and energy dissipation devices. The low-yield-point steel used in this study was tested by Song *et al.* (2015b) to evaluate hysteretic behavior of the shear panel dampers. The yield stress and ultimate strength are assumed to be equal to 105.7 MPa and 247.4 MPa, respectively. A bilinear kinematic hardening model is adopted for steel material, which is more suitable for cyclic loading by taking into account the bauschinger effect. The parameters of E_0, f_y, f_u and ε_y for steel beams were determined to refer to the paper (Wu *et al.* 2016), as listed in Table 1. The stress-strain relationship of steel material was shown in Fig. 11.

In ABAQUS software, the temperature reduction method was adopted to simulate post-tensioned strands in this paper. Based on the principle of heat-expansion and cold contraction, the post-tensioning force can be exerted by applying temperature deduction to the PT strands element, which produces immediately contraction deformation on the element. As a result, the temperature reduction magnitude ΔT is the value of initial force as expected. Setting a temperature T_0 as the initial state, then introduced the temperature T_1 that calculated from T_0 minus ΔT to apply initial post-tension force by causing contraction deformation of PT truss element. The increment ΔT can be determined as follows

$$\Delta T = \frac{F}{\alpha EA} = \frac{\sigma}{\alpha E} \tag{1}$$

where ΔT represents the increment value of temperature; F is the post-tension force; σ is the pre-stressing force; A is the area of post-tensioned strand; E is the elastic modulus of steel strand; α is the coefficient of linear expansion of the

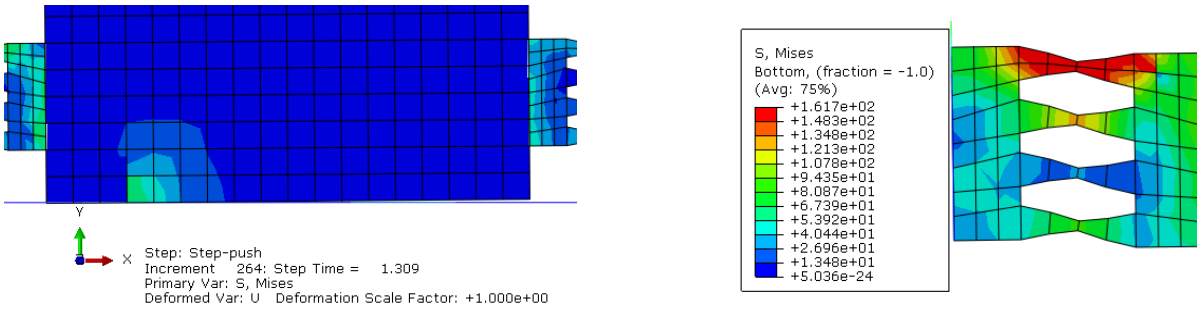

(a) Wall panel starts rocking at 0.2% drift ratio (b) ED devices had yielded at 1% drift ratio

Fig. 13 Typical failure mode of Specimen BASE

post-tension strands, which equals to 1.02×10^{-5}.

The behavior of the concrete was described by adopting concrete damaged plasticity (CDP) mechanical model according to ABAQUS, as shown in Fig. 12. It was suitable for simulating the inelastic behavior of concrete under low confining pressure, monotonic loading, and cyclic loading with the isotropic elastic damage. To describe recovery degree under cyclic loading, weight factor w_t and w_c that related to the properties were used in the model. In this work, the main input parameters, such as d_t and d_c, were defined in accordance to the Chinese Code for design of concrete structures (GB50010 2010).

The boundary conditions were modeled by limiting all nodes of bottom beam from moving and rotating in all directions which means that it is fixed. The reference point at end of top beam was subjected to lateral displacement in X-direction. To model the uplift and rocking of the wall panel, surface to surface contact was defined as the interaction between the concrete wall and the steel frame beam.

Three finite elements available were considered in the model. As a result of the elastic state that panel and beam maintained up to termination of loading, the wall panel can be assumed as a rigid body to simplify the computation caused by constraints of the components. It is simulated by 4-node bilinear plane element CPE4R, which has the characteristic of reduced integration with hourglass control. Besides, a 2-node linear beam in plane B21 element with reduced integration and large-strain formulation, was chosen for the steel frame, energy dissipation devices. The PT strands simulated using 2-node linear truss element T2D2. To improve computational precision, the mesh size of 50 mm is adopted for steel frame beams and wall panel after repeated calculations, and ED devices were assigned to 10 mm to accurately capture the plastic deformation response.

In this paper, loading was applied using a series of analysis steps. Firstly, the strands were given specified initial stress in truss elements by the means of reducing a magnitude temperature. This step also allowed the post-tensioning force transfer into frame beam as a pre-compression. Then, the reference point at beam end was subjected to a displacement controlled lateral load history. The cyclic loading with displacement control was consistent with the test loading system that adopted as depicted in Fig. 6.

3.2 Numerical analysis results

3.2.1 Global behavior

Fig. 13 gives the typical failure mode of Specimen BASE. The wall began isolated from beam when lateral displacement at 0.2% storey drift ratio, as shown in Fig. 13(a). Subsequently, the gap gradually increased and expanded to the compression direction of wall corner as lateral displacement increased, and then the energy dissipation devices begin to yield (see Fig. 13(b)). At 1% storey drift ratio, the complete yield of dampers were observed during rocking of the wall panel. Meanwhile, the steel frame and wall panel were still in elastic stage. As displacement amplitude achieved 2% storey drift ratio, local yielding occurred on the steel beams. Though ED devices had yielded and undertaken major plastic deformation during the loading process, the obvious damage of wall panel has not yet appeared. Finally, the loading stopped at 2.2% roof ratio. It also can be concluded that reasonable frictional interaction is essential to preventing undesirable slip along the wall-beam surface in numerical analysis.

3.2.2 Load-deformation response

In general, the BASE numerical results were observed to have a similar manner to the test results. The hysteretic curve of the whole system is double-flag shape, which shows a self-centering behavior accompanied by favorable energy dissipation capacity. During the whole loading process, three limit states are indicated in the SCWD system, closely match the experimental hysteretic response, as shown in Fig. 14. Before wall panel started rocking, the components were completely in an elastic state with linearly increased bearing capacity. In the AB segment, the hysteresis area in the load-deformation curve is increased as the lateral drift increased. Correspondingly, rotation of the wall panel elongated the PT strands tensioning and the devices had completely yielded at B point (1% lateral drift). The structural stiffness after wall rocking has declined to 1.45 as a results of the stiffness degradation of the devices. Considering that the structural deformation is controllable, the residual bearing capacity of the structural system can be used as a safe reserve.

To further examine the behavior of energy dissipation, the equivalent viscous damping coefficient of the specimen was calculated from the force-displacement hysteresis response for each first cycle. Corresponding to the

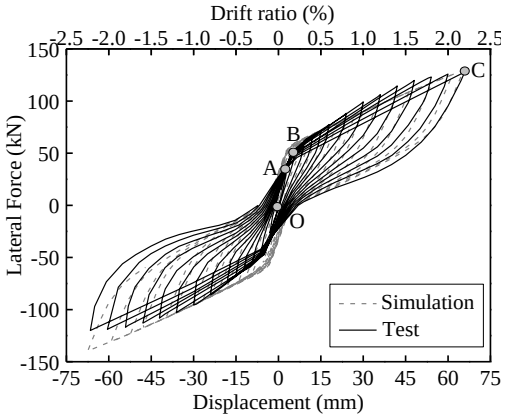

Fig. 14 Load- displacement curves of comparison

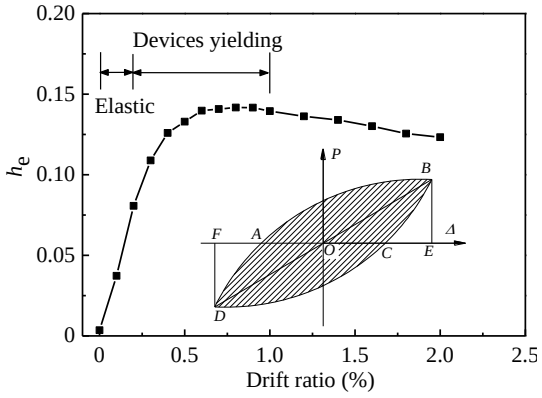

Fig. 15 Equivalent viscous damping coefficient h_e

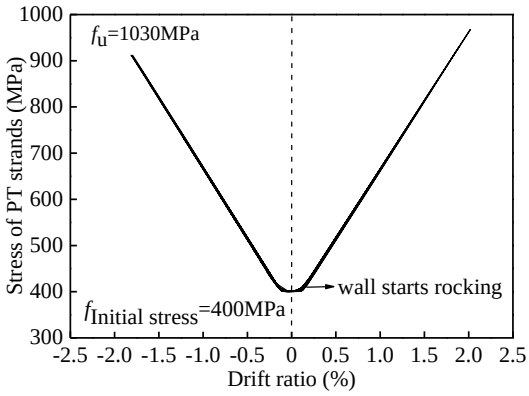

Fig. 16 Hysteretic response of PT strands

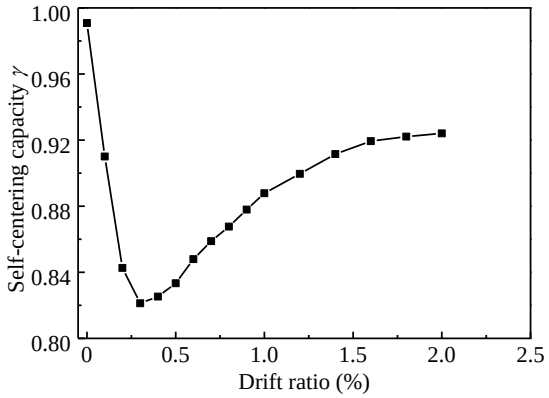

Fig. 17 Self-centering capacity factor γ of BASE

calculation figure that illustrated in Fig. 15, the equation was given in Eq. (2). It is found that the variation trend of h_e is consistent with the failure mode of the frame before devices yielded. Subsequently, h_e is decreased as the displacement increased after ED devices yield.

$$h_e = \frac{S_{(ABC+CDA)}}{2\pi \times S_{(\Delta OBE+\Delta ODF)}} \quad (1)$$

Where $S_{(\Delta ABC+\Delta CDA)}$ is the area inside the lateral force-displacement loop for the module for the given cycle, the area of the effective triangle $S_{(\Delta OBE+\Delta ODF)}$ equal the lateral force strengths multiplied by the absolute values for the relative displacements.

3.2.3 Self-centering performance

Fig. 16 illustrates the lateral drift-stress curve of the PT strands under cyclic loading. σ_0 is the theoretical value of PT strands, which is 50% of the ultimate strength standard value. The PT strands stress increased until lateral displacement reached to 6 mm (0.2% story drift ratio). As the lateral displacement increased, the PT strands stress linearly increased to 985 MPa. The simulation results indicate that the strands are in the elastic state during the process of cyclic loading. The system can be restored to its original state by super-elasticity of PT strands, therefore the structure has good self-centering performance. When the load is reduced to zero, the deformation of the structure is considered as residual drift. A measurement factor, γ is introduced here to account for the self-centering capacity of the structures

$$\gamma = 1 - \frac{\Delta_r}{\Delta_m} \quad (1)$$

where Δ_r and Δ_m are the residual drift after unloading and maximum deformation of each hysteretic cycles, respectively.

Variation of self-centering capacity factor γ related to the drift ratio is indicated in Fig. 17. Before 0.5% lateral drift, energy dissipation mechanism is excited through the yielding of the devices. Meanwhile, a small amount of tensioning in strands due to the slight rotation of wall panel is inadequate for providing restoring moment. As a result, the self-centering capacity γ is decreased. During cycles to 2% lateral drift, γ kept growing since the increased rotation of wall panel elongate the PT strands. Local plastic deformation is finally developed at frame beam, which resulted in a reduction of restoring moment and then residual drift occurs. The residual deformation of the frame is 6.35 mm and the corresponding inter-story drift ratio is only 0.21% at 60 mm maximum lateral displacement. The structure, therefore, has good performance attributed to the limited residual deformation.

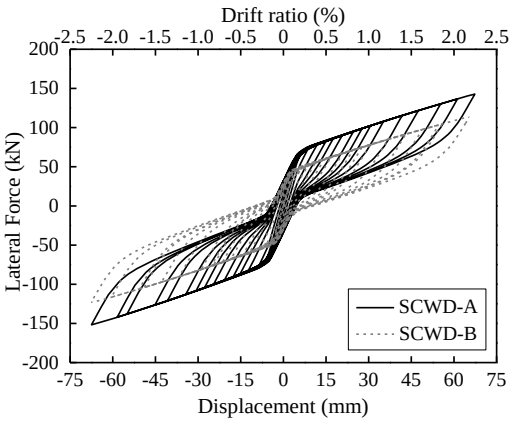

(a) Hysteretic curves

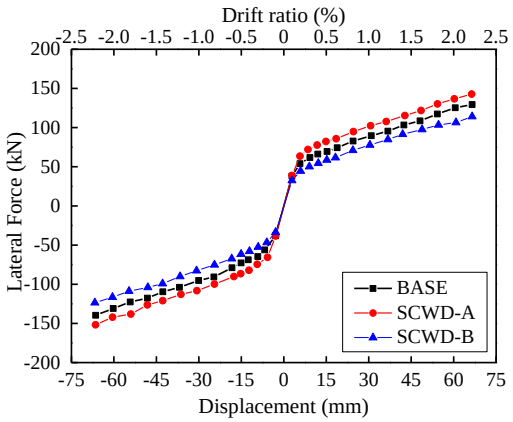

(b) Skeleton curve

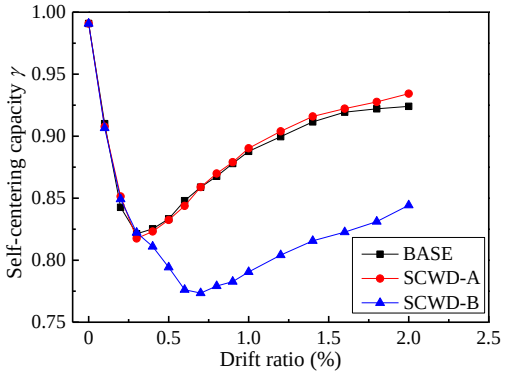

(c) Self-centering capacity factor γ

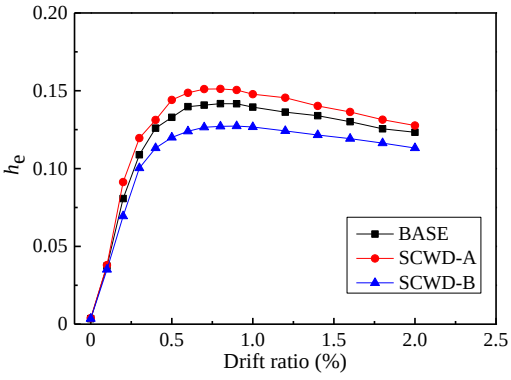

(d) Equivalent viscous damping coefficient h_e

Fig. 18 Effect of the Initial stress of PT strands.

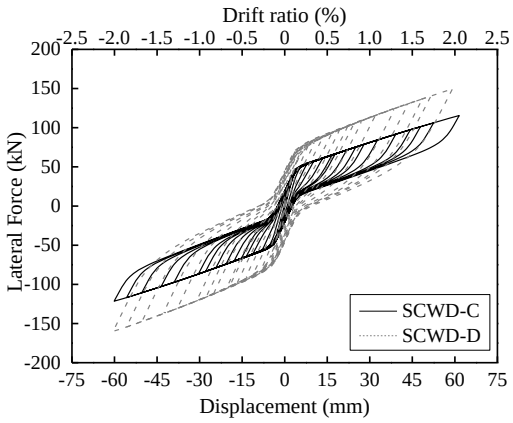

(a) Hysteretic curves

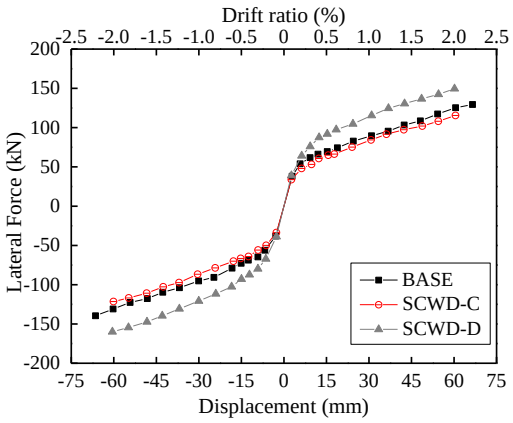

(b) Skeleton curve

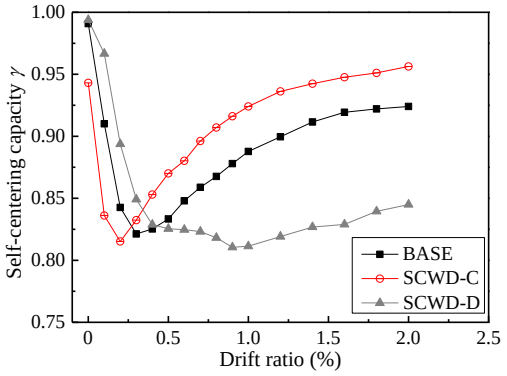

(c) Self-centering capacity factor γ

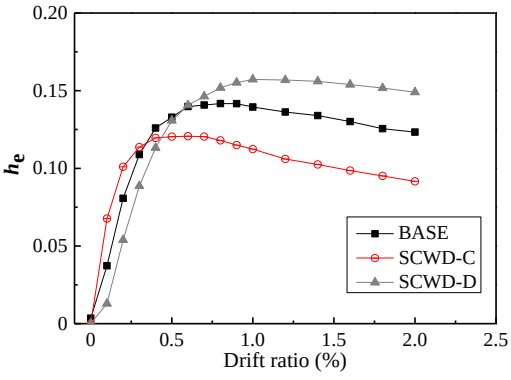

(d) Equivalent viscous damping coefficient h_e

Fig. 19 Effect of yield strength of damper plates

3.3 Parametric studies

Following the numerical analysis described above, a series of specimens were modeled by changing the initial stress of PT strands, the yield strength of damper plates and height-width ratio of the wall. The parametric studies of seven specimens under cyclic loading were conducted to determine the effect on hysteretic behavior of the SCWD structures. Besides, the effectiveness of self-centering capacity and energy dissipation performance were also investigated. A summary of the designed specimens is given in Table 2, which are labeled as A to L beside specimen BASE.

3.3.1 Initial stress of PT strands

The first parametric analysis reported in Table 2 is the initial stress of PT strands. Figs. 18(a)-(b) show the results from load-displacement curves. No significant change observed in initial stiffness of structure until wall begins to rock. The critical load at the point of wall rotation is increased with the increment of initial stress. Note that the stiffness of specimen A and B after the critical point of 0.2% drift ratio are similar to that of BASE specimen. This occurs because the strands and beams maintain elastic until 1% drift ratio is arrived, and consequently provide a steady integral stiffness for the structures after the wall rotated.

From Figs. 18(c)-(d), the self-centering mechanism provided by strands also has a counteractive influence on energy dissipation mechanism. The self-centering capacity factor γ is increased as the rise of initial stress, which exhibit similar trend in comparison to BASE except B with lowest initial stress value. Simultaneously, equivalent viscous dampers are increased though f_{PT} decreased. It is clear that the residual displacement of each specimen at 2% inter-storey drift also increases with the decreased f_{PT}. Therefore, the initial PT stress percentage range from 30% to 60% is favorable to balance the self-centering mechanism and energy dissipation mechanism of the structures.

3.3.2 Yield strength of ED devices

The two cases including C and D were considered to study the effect of the yield strength for plates. Fig. 19(a) demonstrates the specimen with higher yield strength has increased hysteretic area and force capacity. Whether the wall panel rocking or not, the stiffness of the structure is lightly raised as the yield strength increases.

Because of early yielding of the plates, the energy dissipation mechanism is activated in advance before wall rotation at 0.4% lateral drift. However, h_e of specimen C is found to severe declined during cycles to 1% drift ratio. Contrary to the energy dissipation mechanism, the residual deformation of the structure caused by the failure of frame beams finally resulted in the reduction of self-centering capacity. Despite h_e is improved through the yielding of devices, the restoring moment supported by PT strands is excited later so that the structure is insufficient for recovering to original state without damage.

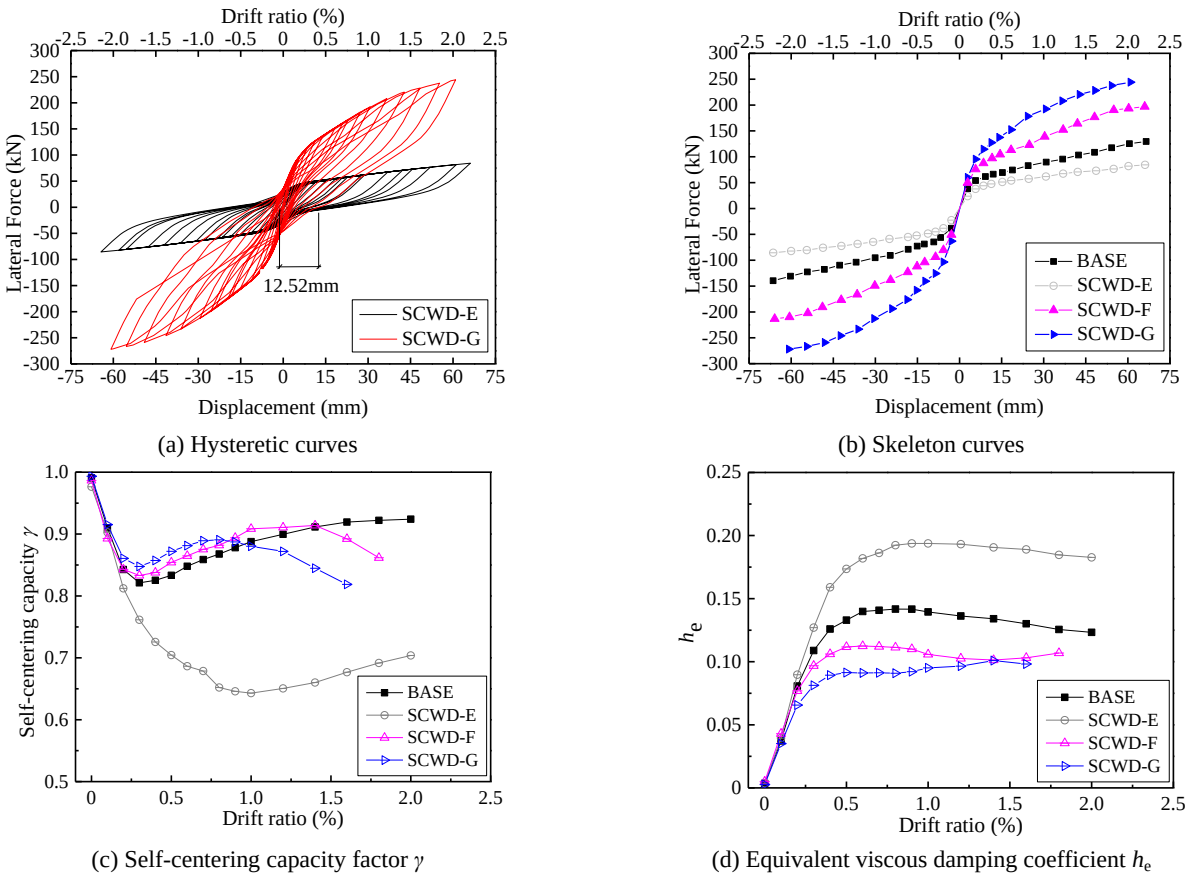

(a) Hysteretic curves

(b) Skeleton curves

(c) Self-centering capacity factor γ

(d) Equivalent viscous damping coefficient h_e

Fig. 20 Effect of height-width ratio of wall panel

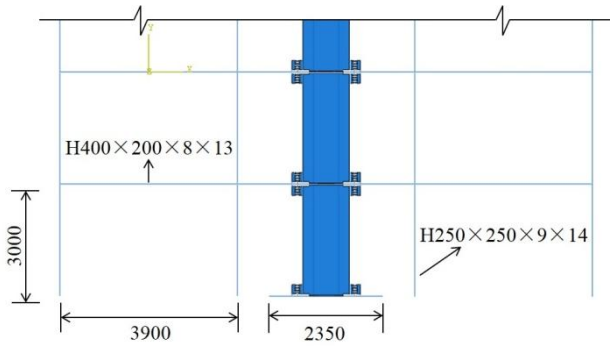

Fig. 21 Simplified model

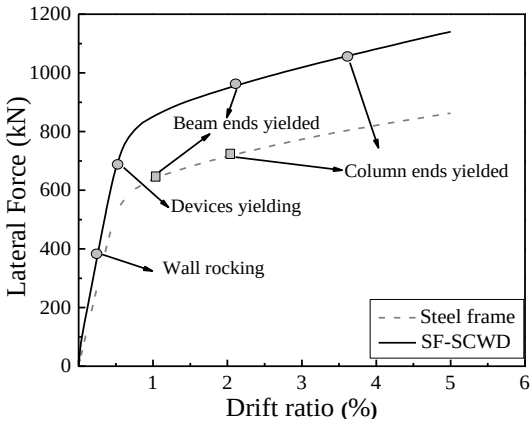

Fig. 22 Monotonic pushover curve

3.3.3 Height-width ratio of wall panel

Another vital consideration discussed in parameter analysis section is height-width ratio *h*/*w* of wall panel, decreasing from 3.19 to 1.82. In Figs. 20(a)-(b), the lateral force-displacement responses of the SCWD-G is compared with that of the SCWD-E. The increased wall width resulted in a noticeable increase in initial stiffness and bearing capacity. The opposite situation is observed when wall width reduced, with decreased lateral strength and hysteresis area. In addition, the stiffness after rotation is gradually decreased owing to large-scale yielding of frame beams.

As *h*/*w* decreased, the increase of vertical displacement after wall rotation elongates the PT strands, which improves the self-centering capacity. After 1% lateral drift, the factor γ gradually reduces since the severe plastic deformation on beams, which resulted in an increase of residual deformation. The residual drift of the structure is highlighted in Fig. 20(a). In addition, the restoring moment provided by self-centering wall in minimum width is less than the lift moment. Then, the structure components provide a significant contribution in dissipating energy by their yielding after plates yielded so that the equivalent viscous damping coefficient remain increases. Consequently, the height-width ratio of wall panel should not exceed 3.5 in order to avoid residual deformations and inadequate energy consumption.

4. Consideration in building

In this Section, static pushover analysis and dynamic numerical simulations of the plane SF-SCWD structure and ordinary steel frame were conducted using ABAQUS. The self-centering wall panel with replaceable energy dissipation devices of steel frame system was considered as a combination of the total steel frame, self-centering wall and devices. The six walls in the middle of the plan were designed as the rocking system. The inter-storey height of 3 m and 3 spans of 3.9 m were assumed in the simplified model of the six-storey prototype building. The beam section H400×200×8×13 and column section H250×250×9×14 were adopted for the frame. The dimension of walls and devices were as same as the BASE specimen, as shown in Fig. 21. The inclusion of embedded section steel in the wall panel was found to have no significant influence on simulation results with respect to the typically seismic behavior of the base model, so it was omitted in order to reduce computational time. The self-centering walls were modeled in the same way as that described above, the beams and columns were modeled as wire beam elements. Besides, the beam density of the models included the mass of floor diaphragms, dead loads and indispensable live loads in the numerical simulations.

4.1 Static pushover analysis

Nonlinear monotonic pushovers used to assess the behavior of the presented system. To deeply understand the failure mechanism, the lateral loads used in the static analyses were proportional to the 5% roof drift, which is far beyond the maximum designed roof drift at 2%. Fig. 22 and 23 show the monotonic pushover results of SF-SCWD and steel frame.

There are two obvious damage characteristics in the steel frame, beam ends yielded, and then a large number of plastic hinges on connections. Differ from the typical failure mode of steel frame, the structure has undergone such a failure process. Firstly, the energy dissipation devices preliminarily yielded at 0.14% roof drift. All devices completely yielded at 0.26% roof drift. Subsequently, the beam ends in the middle layer of the frame began to enter yield state at 0.41% roof drift, followed by the beam plastic hinge and developed to the top of columns. Plastic hinge at beam to column connections occurred at 1% roof drift, and the lateral force at this point is 829.95 kN. PT strands do not yield even the loading displacement continues to increase to 2% roof drift as the beam plastic-hinge rotations drastically. The stress of the PT strands reaches to 960 MPa, which is 88% of the standard value of the ultimate strength.

The ultimate bearing capacity of the SF-SCWD is 1140 kN, it improved 32.2% than that of the steel frame. Also, the stiffness before devices yielding has increased by 33.48%, which is mostly contributed by the walls and devices. The gap between walls and beams also indicate the excellent deformation capacity of the SF-SCWD system. As the most important component in initial energy dissipation, the replaceable energy dissipation devices can substitute for the yielded devices to prevent steel frames from failure.

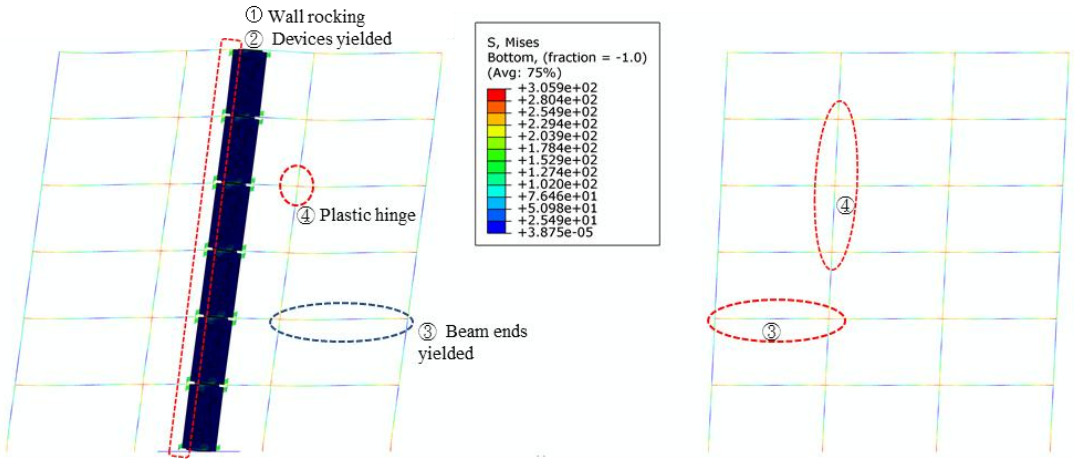

(a) SF-SCWD (b) Steel frame

Fig. 23 Comparison of monotonic pushover results

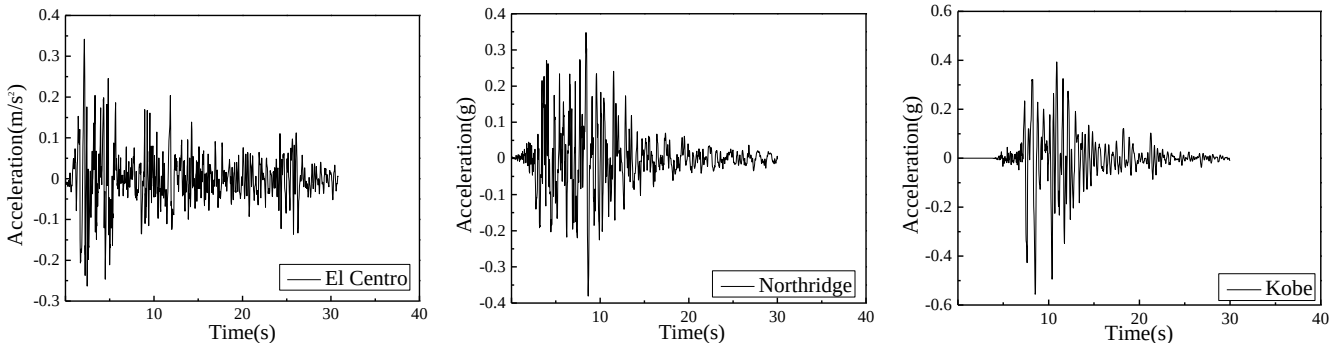

Fig.24 Ground motion records

4.2 Nonlinear time history analysis

In this section, El centro, Northridge and Kobe earthquakes records were chosen to assess the dynamic behavior of the system. The site of the prototype building falls into Site Class II with an average shear wave velocity in the top 30 m of soil, Vs30 (m/s), between 150 m/s and 250 m/s. Three unidirectional ground motion records were selected from the NGA West 2 Ground Motion Database (PEER 2013), as shown in Fig. 24. The records were linearly scaled to match the peak ground acceleration under collapse level earthquakes (exceedance probability of 2% in 50 years). In order to objectively evaluate the actual effect of self-centering wall panel on the residual inter-story drift, free vibration was considered at the end of the earthquake. The selected ground motions were input at the base of the models, which were assumed to be fixed at their base. Following the recommendations in GB50011 (2010), a damping ratio of 5% was assumed in the analysis, implemented using the rayleigh damping model for the first and third vibration modes of structures. The results of nonlinear time history analysis of a 6-story frame are presented here to evaluate the effectiveness of the proposed system in permanent drift mitigation. The considered 6-story frame is shown in Fig. 22, as same as the simplified model in monotonic pushover analysis. The results are compared with the seismic response of ordinary steel frame.

Fig. 25 shows time histories of roof displacement for SF-SCWD structure and steel frames under two excitations. The first natural period of the structure is 0.60 s, whereas the corresponding value for the ordinary steel frame is 0.79 s. As can be seen from Fig. 26, the devices are very effective in suppressing the residual permanent displacement, accounting for approximately 92% under El centro earthquake, 50% for Northridge earthquake and 51% for Kobe earthquake. This is benefited from the displacement-based dampers provide the essential stiffness of the system, which forms a double flag-shaped hysteresis. The self-centering capacity allows the structure revert back to its initial condition during ground motions so that the residual displacement has suppressed. The difference between results originates from different frequency contents of earthquakes.

The maximum interstory drift ratio (IDR) over each story of the frames are illustrated in Fig. 27. As can be seen, the structure has its ideal workability under the three earthquakes. It can be seen from Fig. 27(a) that the maximum IDR decreased up to 41% on the third floor of the SF-SCWD structure when compared to the ordinary steel frames. Similarly, the reduction amounting to 42% can be observed for IDR in the second story under the Northridge earthquake. The elastic-plastic IDR of weak layer Δ_{up} meet the requirements of seismic code (2010) that less than $[\theta_p]h$, where $1/120 \leq \theta_p \leq 1/50$. The post-

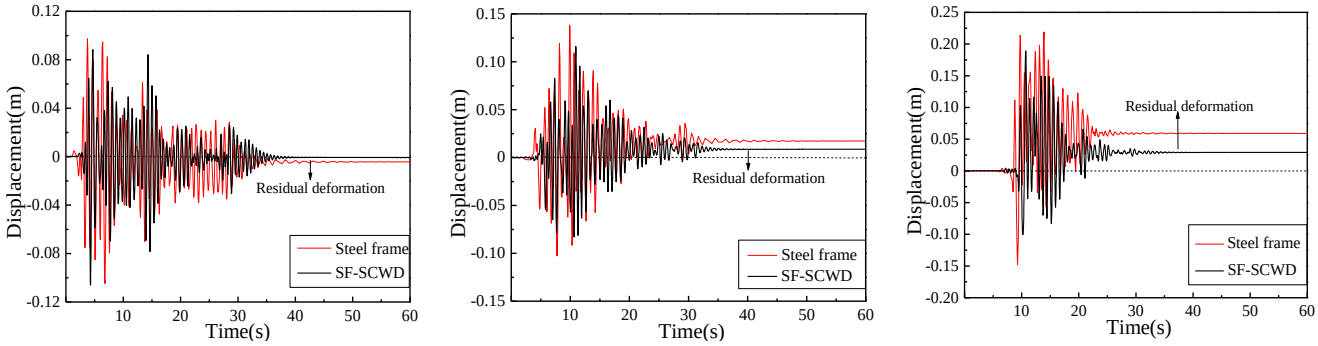

(a) El centro (b) Northridge (c) Kobe

Fig. 25 Displacement and acceleration time histories

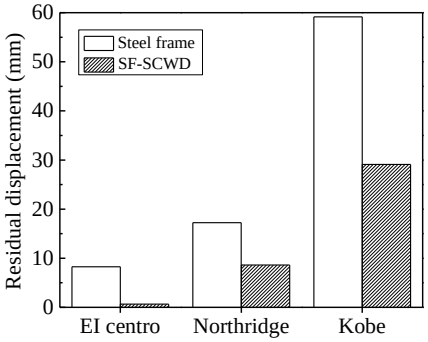

Fig. 26 Comparison of residual displacement

earthquake residual IDA results are shown in Fig. 28. The residual IDA is obviously smaller than that of the steel frame, and the effect of self-centering wall panel during the earthquake is significant. For example, the maximum residual IDA of the first story for steel frame under El centro earthquake is 0.055%, which greatly exceeds the value of SF-SCWD structure. It can be concluded that the energy dissipation devices and PT strands with their higher stiffness and re-centering properties are effective elements in the reduction of residual IDR values.

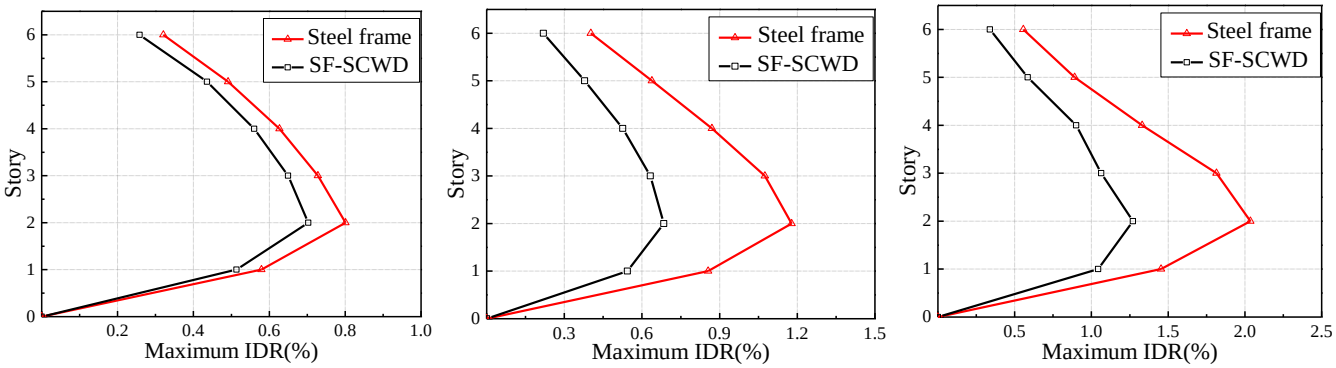

(a) El centro (b) Northridge (c) Kobe

Fig. 27 Maximum interstory drift ratio of steel frame and SF-SCWD

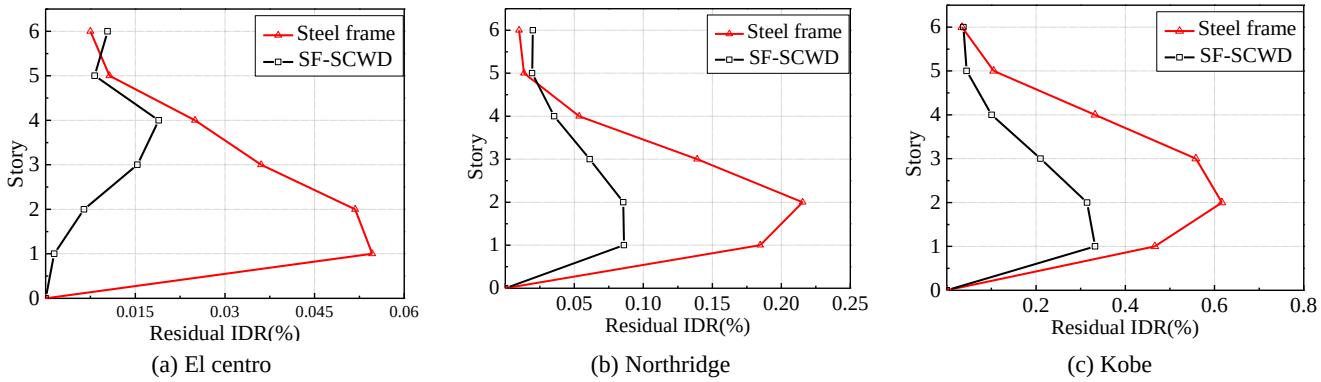

(a) El centro (b) Northridge (c) Kobe

Fig. 27 Maximum interstory drift ratio of steel frame and SF-SCWD

5. Conclusions

This paper presents an innovative steel moment frame with self-centering SRC wall panel incorporating replaceable energy dissipation devices (SF-SCWD). The self-centering RC wall panel utilizes PT strands for providing clamping and restoring forces, and low-yield-point steel plates (LYP) for dissipating energy. Based on the experimental investigation, the FEM was developed to model the cyclic force-displacement of the frames. Furthermore, a parametric study was performed to evaluate the effect of design parameters on the structural characteristics. A six-storey prototype frame with self-centering wall panel and supplemental damping were investigated. Pushover and dynamic analysis were conducted in ABAQUS. Based on the results presented in the paper, the following conclusions are drawn:

- The structures performed an excellent self-centering behavior accompanied by favorable energy dissipation capacity. The PT strands provided re-centering force for wall rotation. The devices continuously dissipated energy during the swing of the self-centering wall panel. The cyclic test results showed that earthquake resilience of the wall panel has the ability to limit structural damage and residual drift, while the energy dissipation devices located at wall toes are used to dissipate energy and reduce the seismic response.
- When initial stress of PT strands increased, the structure response was improved with decreased energy dissipation and reduced returning moment. Limiting the initial stress to less than 50% of ultimate strength will result in a higher equivalent viscous damping coefficient. The increased LYP steel yield strength and plates quantity particularly enhanced the self-centering capacity. The decreased height-width ratio had an opposite influence on residual deformation and stiffness of the structures.
- The results of static pushover analysis showed the three-stage failure procedure of the SF-SCWD structures. Compared with steel frames, the stiffness and bearing capacity of the structures increased by 32.2% and 33.48% than steel frames.
- The time-history analysis results for both steel frame and SF-SCWD structures under different ground acceleration excitation showed that the PT strands and energy dissipation devices were capable of mitigating floor displacement amplitude, maximum interstory drift and residual interstory drift. The reductions of 92%, 50% and 51% of maximum interstory drift were observed in comparison with the drift of steel frames.

Acknowledgments

The research described in this paper was financially supported by Natural Science Foundation of China (No. 51508029), and ‘Fundamental Research Funds for the Central Universities under the research project (No. 30010228971). The supports are gratefully acknowledged.

References

Aaleti, S. and Sritharan, S. (2009), “A simplified analysis method for characterizing unbonded post-tensioned precast wall systems”, *Eng. Struct.*, **31**(12), 2966-2975. https://doi.org/10.1016/j.engstruct.2009.07.024

ABAQUS (2011), Abaqus analysis user’s manual, (Version 6.10), Dassault Systèmes Simulia Corp Providence, RI, USA.

American Concrete Institute (2014), Building code requirements for structural concrete and commentary, ACI 318, Farmington Hills, MI, USA.

American Concrete Institute Innovation Task Group 5 (2007), Acceptance criteria for special unbonded post-tensioned precast structural walls based on validation testing, ACI ITG-5.1-07, Farmington Hills, MI, USA.

Asgarian, B., Salari, N. and Saadati, B. (2016), “Application of intelligent passive devices based onshape memory alloys in seismic control of structures”, *Structures*, **5**, 161-169. https://doi.org/10.1016/j.istruc.2015.10.013

Blebo, F.C. and Roke, D.A. (2015), “Seismic-resistant self-centering rocking core system”, *Eng. Struct.*, **101**, 193-204. https://doi.org/10.1016/j.engstruct.2015.07.016

Chi, H. and Liu, J. (2012), “Seismic behavior of post-tensioned column base for steel self-centering moment resisting frame”, *J. Constr. Steel. Res.*, **78**(11), 117-130. https://doi.org/10.1016/j.jcsr.2012.07.005

Dall’Asta, A., Leoni, G., Morelli, F., Salvatore, W. and Zona, A. (2017), “An innovative seismic-resistant steel frame with reinforced concrete infill walls”, *Eng. Struct.*, **141**, 144-158. https://doi.org/10.1016/j.engstruct.2017.03.019

Deng, K.L., Pan, P., Lam, A., Pan, Z.H. and Ye, L.P. (2013), “Test and simulation of full-scale self-centering beam-to-column connection”, *Earthq. Eng. Eng. Vib.*, **12**(4), 599-607. https://doi.org/10.1007/s11803-013-0200-2

Du, X.L., Wang, W. and Chan, T.M. (2018), “Seismic design of beam-through steel frames with self-centering modular panels”, *J. Constr. Steel. Res*, **141**, 179-188. https://doi.org/10.1016/j.jcsr.2017.11.016

El-Tawil, S., Harries, K.A., Fortney, P.J, Shahrooz, B. and Kurama, Y. (2010), “Seismic design of hybrid coupled wall systems: state of the art”, *J. Struct. Eng.*, **136**(7), 755-769. http://ascelibrary.org/doi/abs/10.1061/9780784410608

GB50010 (2010), Code for design of concrete structures, Ministry of housing and urban-rural development of the People’s Republic of China, Beijing, China. [In Chinese]

GB50011 (2010), Code for Seismic Design of Buildings, Ministry of housing and urban-rural development of the People’s Republic of China, Beijing, China. [In Chinese]

Guo, T., Song, L.L. and Zhang, G.D. (2011), “Numerical simulation of the seismic behavior of self-centering steel beam-column connections with bottom flange friction devices”, *Earthq. Eng. Eng. Vib.*, **10**(2), 229-238. https://doi.org/10.1007/s11803-011-0061-5

Hajjar, J.F. (2002), “Composite steel and concrete structural systems for seismic engineering”, *J. Constr. Steel. Res.*, **58** (5), 703-723. https://doi.org/10.1016/S0143-974X(01)00093-1.

Henry, R.S., Sritharan, S. and Ingham, J.M. (2016), “Finite element analysis of the PreWEC self-centering concrete wall system”, *Eng. Struct.*, **115**, 28-41. https://doi.org/10.1016/j.engstruct.2016.02.029

Ji, X.D., Liu, D. and Hutt, C.M. (2018), “Seismic performance evaluation of a high-rise building with novel hybrid coupled walls”, *Eng. Struct.*, **169**, 216-225. https://doi.org/10.1016/j.engstruct.2018.05.011

Khoshnoud, H.R. and Marsono, K. (2016), “Experimental study of masonry infill reinforced concreteframes with and without corner openings”, *Struct. Eng. Mech., Int. J.*, **57**(4), 641-656.

http://dx.doi.org/10.12989/sem.2016.57.4.641
PEER NGA-West2 Database (2013), Pacific Earthquake Engineering Research Center, Report No. 2013/03. University of California, Berkeley, CA, USA.
Rahgozar, N., Moghadam, A.S. and Aziminejad, A. (2016), "Inelastic displacement ratios of fully self-centering controlled rocking systems subjected to near-source pulse-like ground motions", *Eng. Struct.*, **108**, 113-133. https://doi.org/10.1016/j.engstruct.2015.11.030
Research center for steel structures at Chang'an University (S-CHD) (2019), Cyclic loading tests on substructures of steel frame and self-centering SRC wall panel with energy dissipaters, No. 2019/02, Xi'an, China. [In Chinese]
Saari, W.K., Hajjar, J.F., Schultz, A.E. and Shield, C.K. (2004), "Behavior of shear studs in steel frames with reinforced concrete infill walls", *J. Constr. Steel Res.*, **60**(10), 1453-1480. https://doi.org/10.1016/j.jcsr.2004.03.003.
Song, L.L., Guo, T., Gu, Y. and Cao, Z.L. (2015a), "Experimental study of a self-centering prestressed concrete frame subassembly", *Eng. Struct.*, **88**, 176-188. https://doi.org/10.1016/j.engstruct.2015.01.040
Song, Z.S., Li, J.L., Han, L., Li, H. and Ou, J.P. (2015b), "Experimental study on hysteretic behavior of shear panel dampers made of steel with low yield point", *J. Disaster Prevent. Mitigat. Eng.*, **34**(3), 289-295. [In Chinese]
The San Francisco Planning and Urban Research Association (SPUR) (2009), "The resilient city: defining what San Francisco needs from its seismic mitigation policies", San Francisco, CA, USA.
Tong, X.D., Hajjar, J.F., Schultz, A.E. and Shield, C.K. (2005), "Cyclic behavior of steel frame structures with composite reinforced concrete infill walls and partially-restrained connections", *J. Constr. Steel. Res*, **61**(4), 531-552. https://doi.org/10.1016/j.jcsr.2004.10.002
Twigden, K.M., Sritharan, S. and Henry, R.S. (2017), "Cyclic testing of unbounded post-tensioned concrete wall system with and without supplemental damping", *Eng. Struct.*, **140**, 28-41. https://doi.org/10.1016/j.soildyn.2018.05.007
Vetr, M.G., Nouri, A.R. and Kalantari, A. (2016), "Seismic evaluation of rocking structures through performance assessment and fragility analysis", *Earthq. Eng. Eng. Vib.*, **15**(1), 115-127. https://doi.org/10.1007/s11803-016-0309-1
Wu, H.H., Zhou, T.H., Liao, F.F. and Lv, J. (2016), "Seismic behavior of steel frames with replaceable reinforced concrete wall panels", *Steel Compos. Struct., Int. J.*, **22**(5), 1055-1071. http://dx.doi.org/10.12989/scs.2016.22.5.1055
Zona A., Degee, H., Leoni, G. and Dall'Asta, A. (2016), "Ductile design of innovative steel and concrete hybrid coupled walls", *J. Constr. Steel. Res.*, **117**, 204-213. https://doi.org/10.1016/j.jcsr.2015.10.017

BU